Reversible Electrowetting of Vertically Aligned Superhydrophobic Carbon Nanofibers

Manjeet S. Dhindsa, Neil R. Smith, and Jason Heikenfeld*

Novel Devices Laboratory, University of Cincinnati, Cincinnati, Ohio 45220

Philip D. Rack

Materials Science and Engineering, University of Tennessee, Knoxville, Tennessee 37931

Jason D. Fowlkes, Mitchel J. Doktycz, Anatoli V. Melechko, and Michael L. Simpson

Molecular-Scale Engineering and Nanoscale Technologies Group, Oak Ridge National Laboratory, Oak Ridge, Tennessee 37831

Received April 26, 2006. In Final Form: August 9, 2006

Reversible electrostatically induced wetting (electrowetting) of vertically aligned superhydrophobic carbon nanofibers has been investigated. Carbon nanofibers on a 5×5 μm pitch were grown on Si substrates, electrically insulated with a conformal dielectric, and hydrophobized with fluoropolymer. This nanostructured scaffold exhibited superhydrophobic behavior for saline ($\theta \approx 160°$). Electrowetting induced a contact angle reduction to $\theta \approx 100°$. Competitive two-liquid (dodecane/saline) electrowetting exhibited reversibility on the same nanostructured scaffold. Without applied bias, ultra-fine-point tip (~25 nm radius) nanofibers result in effectively zero capacitance with the overlying saline layer. Complete electrowetting of the substrate is confirmed as capacitance values increase by several orders of magnitude with increased wetting. These results demonstrate the applicability of reversible electrowetting on nanostructured scaffolds and use of nanofabricated structures that can be integrated with various micro- and nanoelectronic technologies.

Introduction

The field of electrowetting[1] continues to rapidly expand in applications ranging from lab-on-chip,[2] liquid lenses,[3] and displays[4,5] to microelectromechanics.[6] After recent demonstrations of electrowetting on a superhydrophobic nanostructured surface,[7] further investigations are needed in techniques for generating wetting reversibility, methods for measuring wetting state, use of integration with nanofabrication methods, competitive two-liquid oil/saline electrowetting, and gradual electrowetting response (i.e., not a step function). We are investigating competitive two-liquid dodecane/saline electrowetting on nanostructured surfaces for use in novel optical and biomedical devices. We report here electrowetting on vertically aligned carbon nanofibers (CNFs).[8] Integration with standard nanofabrication techniques, gradual electrowetting, capacitance measure of wetting state, and reversible dodecane/saline electrowetting are also reported. Demonstrated wetting transitions (Figure 1) include irreversible superhydrophobic to wetted and reversible two-liquid (dodecane/saline) competitive electrowetting.

Experiment Section

Standard nanofabrication processes were used to create a superhydrophobic scaffold on Si substrates. The CNFs were grown in 5×5 micrometer arrays using a DC plasma-enhanced chemical vapor deposition process (DC−PECVD). This is a catalytically driven process where the lithographically defined Ni catalyst particles serve as localized sites for nanofiber growth. Details on the patterning and growth process for the CNFs have been previously reported.[9] The average CNF height is ~10 μm. The CNFs are electrically conductive and serve as a fine-tipped ground electrode (~25 nm avg. tip radius). As shown in Figure 1 and in the SEM photos of Figure 2, for comparative purposes the CNFs were insulated using two different conformal coating processes. For one sample set, ~200 nm Al_2O_3 ($\epsilon_r \approx 9$, $E_{bd} \approx 7.6$ MV/cm) was coated using a Cambridge NanoTech atomic layer deposition (ALD) tool. The ~300 °C ALD process utilizes alternating pulses of trimethylaluminum and H_2O vapors.[10] Unlike carbon nanotubes, the CNF surfaces have numerous surface defects for uniform nucleation of Al_2O_3 growth. For a second sample set, ~1.1 μm of organic Parylene C ($\epsilon_r \approx 3$, $E_{bd} \approx 2$ MV/cm) coating was deposited using a Specialty Coating Systems 2010 Lab-Coater. This process involves dimer vaporization and vapor pyrolysis followed by room-temperature monomer deposition and polymerization on the substrate surface at ~0.1 Torr. Due to the lower electrical breakdown field of Parylene, a Parylene coating thicker than that for Al_2O_3 was implemented. The differing capacitance value for Parylene vs Al_2O_3 was also useful for further testing the experimental conclusions. Both samples were further hydrophobized using a solution coating of 1 wt % fluoropolymer in fluorosolvent, such as DuPont Teflon AF Grade 400S1-100-1 in 3M Fluorinert. After fluorosolvent removal and oven curing at ~160 °C, the resulting coated CNFs have a surface energy of $\gamma \approx 14$ mN/m. The fluoropolymer coating ($\epsilon_r \approx 2.1$, $E_{bd} \approx 1$ MV/cm) is conformal but not as uniform in thickness (~200−400 nm) as the dielectric coating processes.

* To whom correspondence should be addressed. E-mail: heikenjc@email.uc.edu.

(1) Mugele, F.; Baret, J. *J. Phys. Condens. Matter* **2005**, *17*, 705.
(2) Pollack, M. G.; Fair, R. B.; Shenderov, A. D. *Appl. Phys. Lett.* **2000**, *77*, 1725.
(3) Berge, B.; Peseux, J. *Eur. Phys. J. E* **2000**, *3*, 159.
(4) Hayes, R. A.; Feenstra, B. J. *Nature* **2003**, *425*, 383.
(5) Heikenfeld, J.; Steckl, A. J. *Appl. Phys. Lett.* **2005**, *86*, 011105.
(6) Lee, J.; Kim, C. *J. Micromech. Syst.* **2000**, *9*, 171.
(7) Krupenkin, T.; Taylor, J. A.; Schneider, T. M.; Yang, S. *Langmuir* **2004**, *20*, 3824.
(8) Melechko, A. V.; Merkulov V. I.; McKnight, T. E.; Guillorn, M. A.; Klein, K. L.; Lowndes, D. H.; Simpson, M. L. *J. Appl. Phys.* **2005**, *97*, 041301.
(9) McKnight, T. E.; Peeraphatdit, C.; Jones, S. W.; Fowlkes, J. D.; Fletcher, B. L.; Klein, K. L.; Melechko, A. V.; Doktycz, M. J.; Simpson, M. L. *Chem. Mater.* **2006**, *18*, 3203.
(10) Biercuk, M. J.; Monsma, D. J.; Marcus, C. M.; Becker, J. S.; Gordon, R. G. *Appl. Phys. Lett.* **2003**, *83*, 2405.

10.1021/la061139b CCC: $33.50
Published on Web 09/15/2006

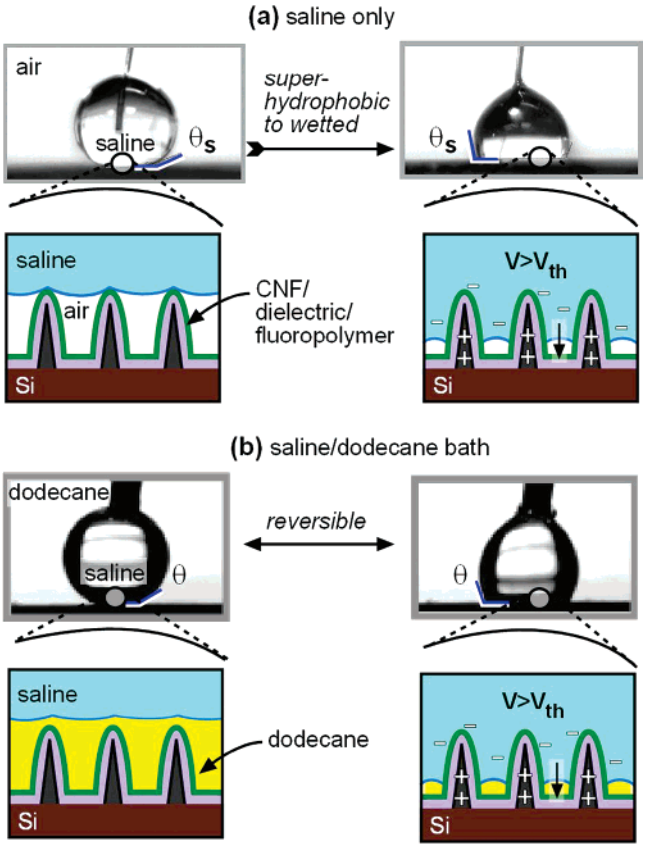

Figure 1. Electrowetting on vertically aligned carbon nanofibers (CNFs) coated with dielectric and hydrophobic fluoropolymer: (a) saline/air electrowetting of superhydrophobic surface, (b) the same surface exhibiting reversible electrowetting for a saline/dodecane system. The droplet electrode in b was larger in order to better control positioning of the droplet in the dodecane bath.

The saline solution used for electrowetting was comprised of 80 wt % deionized water ($\gamma \approx 73$ mN/m), 19.99 wt % glycerin ($\gamma \approx 64$ mN/m, Fisher, >99.5% purity), and 0.01 wt % KCl (Fisher, >99% purity). The resulting surface tension for this saline mixture is ~70 mN/m. For the saline/air experiments, the purpose of the glycerin was to reduce evaporation rate during data acquisition. Although not required for the saline/oil-bath experiments, the same glycerin content was utilized for consistency in experimentation. In an applications environment, a hermetic top plate would be provided and the need for glycerin eliminated. KCl increases the solution conductivity and decreases the aqueous Debye length to ~10 nm. The pinhole-free nature of the Parylene and Al_2O_3 coatings prevent electrochemical reaction of the saline with the carbon nanofibers. Electrically insulating dodecane oil ($\gamma \approx 25$ mN/m, Acros, >99% purity) was utilized as a second liquid in competitive electrowetting testing. Contact angles were measured using an AST VCA-Optima surface analysis system. The system uses automated gray-scale imaging and performs a droplet curve-fit and baseline determination to calculate the contact angle. An electrical potential was applied to a sessile saline droplet by insertion of a Ni/Ti wire electrode. The bottom of the Si substrate was electrically grounded, and as a result, the CNFs were electrically grounded as well.

Discussion

The contact angle for a three-phase solid(S)−liquid(L)−vapor-(V) system on a planar substrate is predicted by interfacial surface tension (γ) according to Young's equation[1]

$$\cos \theta_P = \frac{\gamma_{SV} - \gamma_{SL}}{\gamma_{LV}}, \qquad (1)$$

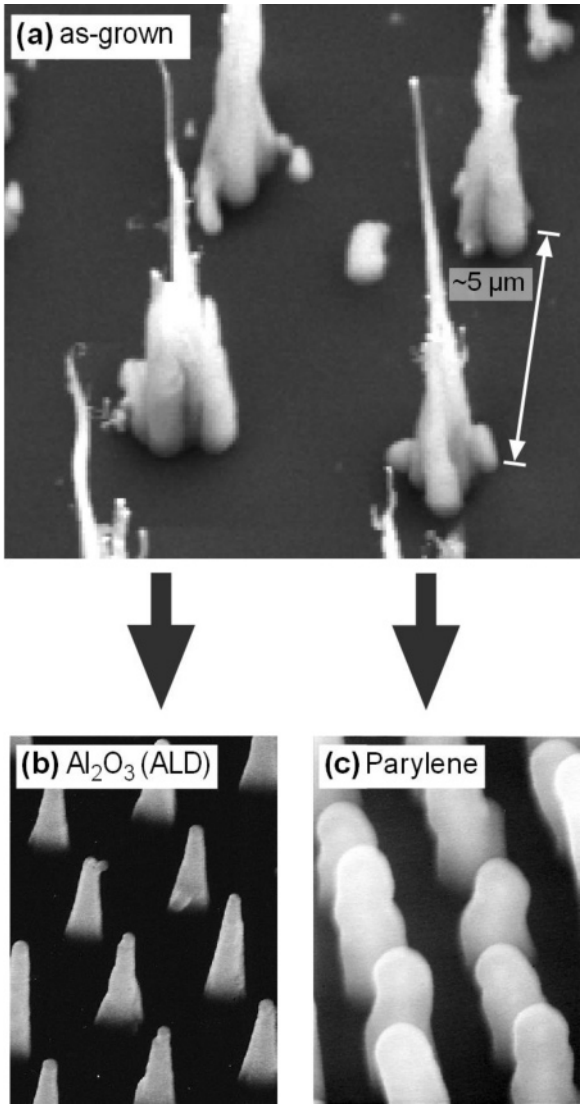

Figure 2. Scanning electron micrograph of CNFs on a 5 × 5 μm pitch (a) as grown, (b) conformally coated with atomic layer deposition of ~200 nm Al_2O_3, and (c) coated with ~1.1 μm of Parylene C. The CNF (electrode) growth process terminates with a nanoscale (~25 nm) tip radius.

For a system where the vapor phase is replaced with oil (dodecane), interfacial surface tension terms in eq 1 are substituted with oil instead of vapor. For the fluoropolymer coating and saline used in this work, θ_p is ~115°. For a structured surface, this equation is insufficient. The contacting liquid experiences an 'average' surface energy of the contacting solid and the space between the structures (air, or a second immiscible liquid). Given the approximately zero surface energy of air and a fractional area occupied by the tips of the high aspect ratio CNFs, superhydrophobicity (θ > 150°) for polar water arises according to the Cassie−Baxter relation

$$\cos \theta_S = \beta(\cos\theta_P + 1) - 1, \qquad (2)$$

where θ_S is the structured surface contact angle (Figure 1), θ_P is the contact angle for the same solid in continuous planar format, and β is the fractional contacting area between the liquid and solid. However, the coated CNF tops are hemispherical and therefore complicate an exact predictive calculation for the macroscopically observed droplet contact angle. At the microscopic level, eq 1 is most important for the experiments reported

here. This is because capillary wetting of the saline between the CNFs occurs when the saline meniscus transitions from a convex shape to a concave shape via electrowetting (Figure 1). The meniscus curvature is determined by the side-wall contact angle, which is determined by eq 1.

For both saline/air and saline/dodecane systems the saline does not wet the inter-CNF space at zero voltage (no electrowetting). However, for the saline/dodecane system the inter-CNF space is occupied at zero voltage by the dodecane (Figure 1b). The lower surface tension of the nonpolar dodecane causes it to readily occupy the space between the low-surface energy CNFs. For this system interfacial surface tensions predict a saline droplet contact angle of 180° for both a planar and a structured surface.[1] The lower measured value of 160° is due to gravitational force, a slight force of the wire electrode, and/or error due to the resolving limits of the contact angle measurement system and associated software.

For the electrowetted system, according to the Lippman electrocapillary effect adapted to a dielectric, effective interfacial surface tension, between the saline and the fluoropolymer should decrease according to

$$\gamma_{SL}(V) = \gamma_{SL}(0) - \frac{\epsilon}{2 \cdot z}(V)^2, \qquad (3)$$

where $\gamma_{SL}(V)$ is the solid−liquid interfacial surface tension as a function of applied voltage, $\gamma_{SL}(0)$ is the solid−liquid interfacial surface tension at zero voltage, and ϵ/z is an effective dielectric constant and thickness for the series capacitance of the dielectric/fluoropolymer coating. Equation 3 can be combined with eq 1 to create the so-called electrowetting equation

$$\cos\theta(V) = \cos\theta_{V=0} + \frac{\epsilon}{2 \cdot z \cdot \gamma_{LV}}(V)^2 \qquad (4)$$

It is important to note that the interpretation of electrowetting provided by eqs 3 and 4 is only one of several models for electrowetting behavior.[1] For a planar surface, eq 4 can predict the saline contact angle up to the point of contact angle saturation. Contact angle saturation at ∼50−70° occurs for a variety of reasons such as charge injection into the fluoropolymer.[1]

For a uniformly structured surface, such as one comprised of perfectly perpendicular and flat-top pillars, one would expect and witness[7] a nearly instantaneous transition ($\Delta V < 5$ V) between a superhydrophobic state and capillary wetting into the interpillar spaces. This immediate transition is due to high geometrical uniformity for the pillar platform. As the contact angle at the pillar side-wall/saline interface is reduced to below 90° (i.e., concave meniscus), capillary electrowetting occurs between all the pillars. This experiment and theory has been previously reported by Krupenkin et al.[7]

For the devices reported here, a *gradual* wetting response is witnessed for both sample sets and in both air and dodecane environments (Figure 3a). Similar to the pillar platform,[7] as the saline transitions to a concave meniscus with increasing voltage (Figure 1, right), capillary wetting occurs. However, for the CNF platform reported here, geometrical variations between individual CNFs broaden the contact angle vs voltage response. For example, CNFs side walls with differing degrees of side-wall slope will have different threshold voltages for capillary wetting (i.e., transition between a convex/concave meniscus). The gradual response is also partially attributed to rounded CNF tips which provide a gradual geometrical transition from the CNF tip to the capillary geometry between the CNFs. This gradual electrowetting response is advantageous for applications such as electrooptics[3,4] in which modulation of the macroscopic droplet profile is desired.

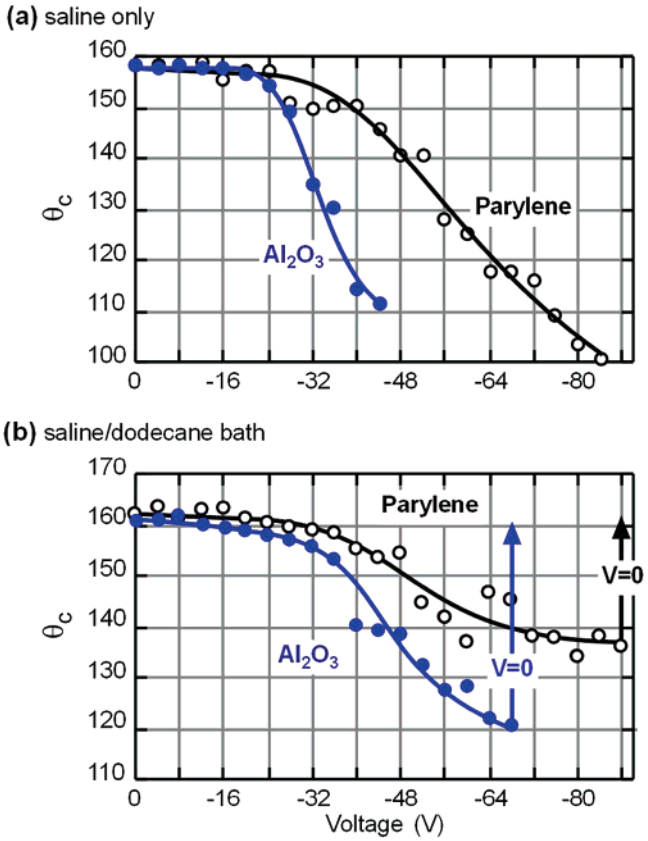

Figure 3. Contact angle vs voltage for (a) saline/air and (b) saline/docecane bath. In a, after the voltage is removed the droplet remains wetted at the measured contact angle. In b, removing the voltage returns the droplet to the initial contact angle before voltage was applied. Each set was taken to near the point of contact angle saturation.

The Al_2O_3-coated CNFs achieve electrowetting at ∼10's of volts less than the Parylene samples. This is likely due to the combined influence of dielectric capacitance and side-wall slope. The samples with Al_2O_3/fluoropolymer coating have higher capacitance (eqs 3 and 4: larger ϵ_r, reduced z). This expectation of decreased operating voltage is consistent with previous work that compared the electrowetting of Parylene to lower voltage electrowetting of higher capacitance metal oxides dielectrics with a thin fluoropolymer top coat.[11] Lowering of electrowetting voltage is also due to the geometrical differences seen in the coated CNF photographs of Figure 2 b,c. The Parylene-coated CNFs have, on average, fairly vertical side walls. A side-wall slope of ∼80−85° is visible for the Al_2O_3-coated CNFs. This reduces the voltage required for a transition between a convex and concave meniscus. From eq 4, this voltage reduction is only on the order of 5−10 V. This further supports increased capacitance contributing most to the decreased voltage requirement for the Al_2O_3-coated CNFs.

An important comparison should also be made between electrowetting of CNFs in an air vs oil environment. Electrowetting in an air environment is *irreversible* (Figure 3b). When the voltage is removed (grounded) the saline/air system remains at the electrowetted contact angle. This is because the system should remain in a state of minimum energy (minimum interfacial surface energy). For the two-liquid saline/dodecane system, the

(11) Moon, H.; Cho S. K.; Garell, R. L.; Kim, C. J. *J. Appl. Phys.* **2002**, *92*, 4080.

wetting behavior is *reversible* at all wetting states. When the voltage is removed (grounded) the saline/dodecane system returns to the initial contact angle observed at zero voltage. This is due to interfacial surface tension forces between the dodecane/saline and dodecane/fluoropolymer which cause capillary filling of the inter-CNF space under thermal equilibrium conditions ($V = 0$). Interfacial surface tensions also cause the contact angle of 180° in most oil/saline/fluoropolymer systems (i.e., the oil forms a film between saline and fluoropolymer). For both Al_2O_3 and Parylene sample sets, the time scale for the reversible contact angle change on the CNFs was slow (1 to 3 s) compared to that witnessed for the same liquids on a planar surface (10's to 100's ms). This is likely due to metastable pinning effects on the rough surface produced by the CNFs.

Capacitance vs voltage measurements for both saline/air and saline/dodecane were recorded in order to provide direct evidence of wetting into the inter-CNF space. A ~pF capacitance meter was insulated from the applied DC voltage source using an external capacitor. The capacitance meter uses a small-signal AC waveform to measure capacitance. Therefore, the capacitance of the voltage source was isolated from the measurement setup by also including a 1 MΩ resistor at the voltage source output. The wafer/CNF capacitance can be theoretically estimated to be the sum of the coated Si base (C_P), the coated CNF side walls approximated as cylinders or cones (C_C), and the hemispherical coated CNF tips (C_S)

$$C_P = \frac{\epsilon A}{z},\ C_C = \frac{2\pi\epsilon h}{\ln(r_o/r_i)},\ C_S = \frac{4\pi\epsilon}{1/r_i - 1/r_o} \qquad (5)$$

where r_o and r_i are the outer and inner radii for the dielectric/fluoropolymer coating on the CNFs. The maximum achievable capacitance (F) via electrowetting is comprised of two components. The first is due to the CNFs and is found by multiplying C_C and C_S by the contacting droplet area and the density of CNFs per unit area ($4 \times 10^{10}/m^2$). The second is due to the Si substrate and is found by multiplying C_P by the contacting droplet area. As shown in Figure 4 for low voltages, the capacitance for the dewetted (superhydrophobic) state (C_S) is effectively zero. This is because the nanoscale CNF tips ($r_i \sim 25$ nm) result in a very small C_S (eq 5). If the saline fully electrowets the space between the CNFs, the measured capacitance should be $C_C + C_S + C_P$. This maximum capacitance is calculated to be ~10's pF for the Parylene samples and ~100's pF for the Al_2O_3 samples. This is consistent with the maximum measured capacitance values in Figure 4a,b. This implies that in the experiments if sufficient voltage was provided, the majority of air (Figure 4a) or dodecane (Figure 4b) was pushed out of the inter-CNF space.

A gradual increase in capacitance is observed with increasing voltage for both Al_2O_3 and Parylene sample sets and both saline/air and saline/dodecane systems. The gradual capacitance increase is due to the same effects causing a gradual contact angle increase. To reiterate, the geometrical variation of the CNFs, particularly the CNF side-wall slopes, causes variation in the threshold voltage for capillary wetting. If all CNF's were of identical geometry and had a straight-line side-wall slope, one would expect a nearly instantaneous increase in capacitance at a single threshold voltage for capillary wetting into the CNF array. This could be achieved using etching of Si posts[7] instead of growing CNFs. However, additive fabrication techniques such as CNF growth provide potential advantages such as integration on existing semiconductor devices.

Eventually the capacitance increase with voltage begins to saturate. On the basis of the previous discussion, this implies that the majority of air or dodecane is pushed out of the inter-CNF space. The capacitance and voltage data are quite different between the Al_2O_3 and Parylene sets. Even so, the stored energy densities (CV^2) near saturation for all data sets are comparable (~10's mJ/m^2). The storage energy density is directly related to a decrease in saline contact angle with the CNF side walls (eqs 3 and 4). The similarity of the stored energy densities for all data sets roughly support the expectation that full capillary wetting of the inter-CNF space should occur at similar energy densities. That is, Al_2O_3 and Parylene sample sets have similar geometry and should therefore experience capillary wetting at a similar reduction in effective interfacial surface tension (eq 3).

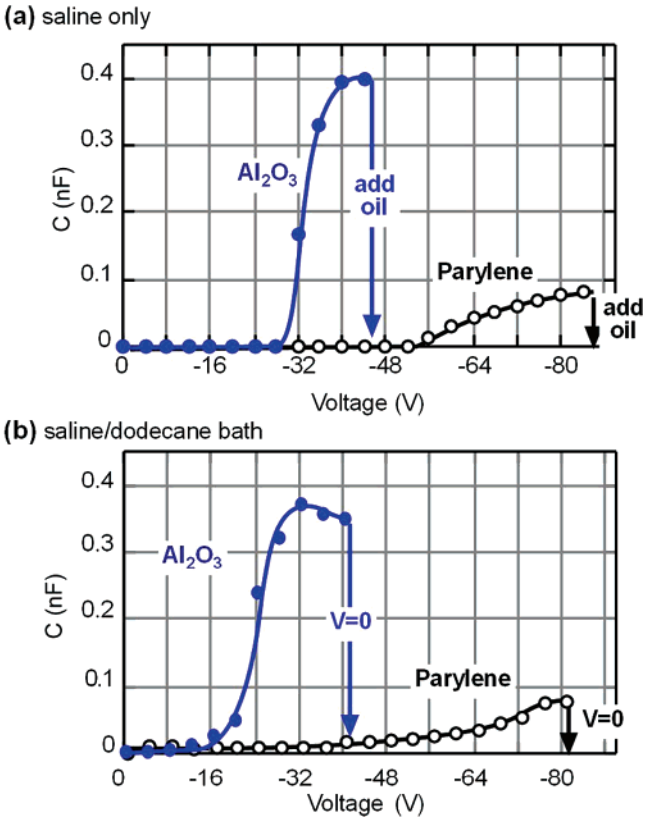

Figure 4. Capacitance vs voltage for electrowetting of (a) saline/air and (b) saline/docecane bath. Stored energy density at approximately full wetting of the inter-CNF space is labeled at the end of each curve. For a, addition of oil at the end of each experiment caused the water to dewet and the capacitance to return to ~0 nF. For b, after achieving any wetting state, removing the applied voltage caused the capacitance to return to ~0 nF.

For the saline/air system, dodecane was also dosed onto the top of the wetted droplet *after* electrowetting was achieved (Figure 4a). The dodecane was observed to encompass the droplet near the contact line, but gravitational effects (absence of a supporting dodecane bath) prevent a macroscopically observable change in contact angle. However, as expected, addition of dodecane caused the capacitance to immediately return to about zero. This further confirms that the dodecane occupies the inter-CNF spaces at zero voltage. The time scale for capacitance decrease was rapid (<1 s). Therefore, the low viscosity of dodecane and saline (both <2 cSt) allows for ease of fluid flow horizontally through the array of CNFs. Despite the expectation of electric field enhancement at the ultrahigh-aspect ratio CNF tips, water electrolysis was not observed during testing. This confirms robust dielectric insulation of the CNFs. The insulation was so reliable that after electrically charging and inducing wetting for the saline/dodecane/CNF system, the bias electrode could be removed and the droplet would retain its capacitance value.

Summary

In summary, electrowetting of vertically aligned CNFs was investigated. Superhydrophobic ($\theta_s \approx 160°$) wetting behavior for water was demonstrated. Standard nanofabrication methods were utilized for fabricating the superhydrophobic scaffolds which are compatible with integration of electronic devices. Electrowetting experiments show a gradual decrease in contact angle to $\theta \approx 100-110°$. Competitive two-liquid electrowetting exhibited reversible behavior. Experimental capacitance measurements were also shown to validate wetting states. These results on nanostructured scaffolds advance electrowetting toward our working-group's long-term goals of novel and improved electrooptics, lab-on-chip, and biomedical devices.

Acknowledgment. Primary financial support for this project at the University of Cincinnati was provided by a UC Research Council award. The ORNL authors acknowledge support from NIH grant EB000657 and from the Center for Nanophase Materials Sciences. A.V.M. and M.L.S. acknowledge support from the Material Sciences and Engineering Division Program of the DOE Office of Science. The authors thank Dr. J. S. Becker of Cambridge NanoTech Inc. for providing the ALD coatings.

LA061139B